nature
physics

Light emission based on nanophotonic vacuum forces

Nicholas Rivera [1]*, Liang Jie Wong[2,3], John D. Joannopoulos[1], Marin Soljačić [1] and Ido Kaminer [4]*

The vanishingly small response of matter to light above ultraviolet frequencies makes the manipulation of light emission at such frequencies challenging. As a result, state-of-the-art sources of high-frequency light are typically active, relying on strong external electromagnetic fields. Here, we present a fundamental mechanism of light emission that is fully passive, relying instead on vacuum fluctuations near nanophotonic structures. This mechanism can be used to generate light at any frequency, including high-frequency radiation such as X-rays. The proposed mechanism is equivalent to a quantum optical two-photon process, in which a free electron spontaneously emits a low-energy polariton and a high-energy photon simultaneously. Although two-photon processes are nominally weak, we find that the resulting X-ray radiation can be substantial. The strength of this process is related to the strong Casimir–Polder forces that atoms experience in the nanometre vicinity of materials, with the essential difference being that the fluctuating force here acts on a free electron, rather than a neutral, polarizable atom. The light emission can be shaped by controlling the nanophotonic geometry or the underlying material electromagnetic response at optical or infrared frequencies. Our results reveal ways of applying the tools of nanophotonics even at frequencies where materials have an insubstantial electromagnetic response. The process we study, when scaled up, may also enable new concepts for compact and tunable X-ray radiation.

Since the early days of quantum mechanics, quantum vacuum fluctuations have been a constant source of fascination. The non-zero energy density of the vacuum gives rise to a wide variety of important physical effects that continue to be subjects of intense theoretical and experimental research. In the case of the quantized electromagnetic field, key examples of these effects include spontaneous emission[1], Lamb shifts[2], Casimir(–Polder) and van der Waals forces[3–5], quantum friction[6], the dynamical Casimir effect[7,8] and the Unruh effect[9–11].

A paradigm that has taken hold in recent years is control over these vacuum effects by either nanostructuring of the electromagnetic modes of optical materials[12] or using nanoconfined electromagnetic modes in materials with negative permittivity or permeability[13,14]. This paradigm works because the electromagnetic modes control the spatial and spectral properties of the electromagnetic vacuum. A well-studied example of these concepts is the Purcell effect[15], in which the modification of the local density of states of the electromagnetic field alters light emission by stationary or moving atoms[16,17] and free electrons[18–22]. Another example would be the control of Casimir forces and related phenomena, such as near-field radiative heat transfer, which are attributed to fluctuating electromagnetic fields near optical materials. These effects are very strong when two optical materials are a few nanometres away from each other, due to the very large field fluctuations associated with the nanoscale. The large field fluctuations motivate the strong theoretical[23–27] and experimental[5,28–30] push to observe these effects using nanoscale gaps between materials.

Controlling the electromagnetic vacuum ceases to be simple at high frequencies, typically beyond the ultraviolet (UV) range[31]. This is a direct consequence of the fact that in almost all known materials, the permittivity approaches that of vacuum at these high frequencies. As a result, the generation of high-frequency radiation

(hard UV through gamma rays) from emitters relies on the presence of static or dynamic external fields, as in light-generation processes used in synchrotrons, laser undulators, and free-electron lasers[32–36]. Alternatively, the radiation can come from the weak dielectric response of materials at very high frequencies, as in parametric X-ray generation[37]. The very weak material response at very high frequencies seems to preclude using ideas from nanophotonics and materials physics to influence high-frequency radiation.

Here, we show how electromagnetic vacuum fluctuations at infrared (IR) and visible frequencies near and inside materials can be used as a means of controlling light emission at very high frequencies, such as X-rays. The mechanism that we propose to exert such control is a two-quantum process involving the spontaneous emission of a photon and a polariton by an energetic free electron (Fig. 1). Although two-quantum (spontaneous) emission processes are second-order processes in quantum electrodynamics (QED) and are thus considered very weak, the large strength of vacuum forces in the nanoscale vicinity of materials nevertheless leads to a strong per-electron power emitted into high-frequency radiation. In fact, we find that the radiated power is comparable with that emitted by an equal-energy electron moving in an externally applied magnetic field of strength on the order of 1 T. Due to the high spatial confinement of the emitted polariton, the intensity of the emitted light is substantial at higher frequencies than in many known light sources, even when modest electron energies are used in our scheme.

For example, in comparison with current X-ray free-electron lasers and synchrotrons that utilize GeV-energy electrons to produce few-kiloelectronvolt X-rays, an X-ray output of 5 keV can be achieved with electron kinetic energies of about 5 MeV and gamma-ray output of 50 MeV can be achieved with electron kinetic energies of around 500 MeV. The emission is broadband, potentially enabling applications in probing physics from UV to hard

[1]Department of Physics, Massachusetts Institute of Technology, Cambridge, MA, USA. [2]Singapore Institute of Manufacturing Technology, Singapore, Singapore. [3]School of Electrical and Electronic Engineering, Nanyang Technological University, Singapore, Singapore. [4]Department of Electrical Engineering, Technion, Haifa, Israel. *e-mail: nrivera@mit.edu; kaminer@technion.ac.il
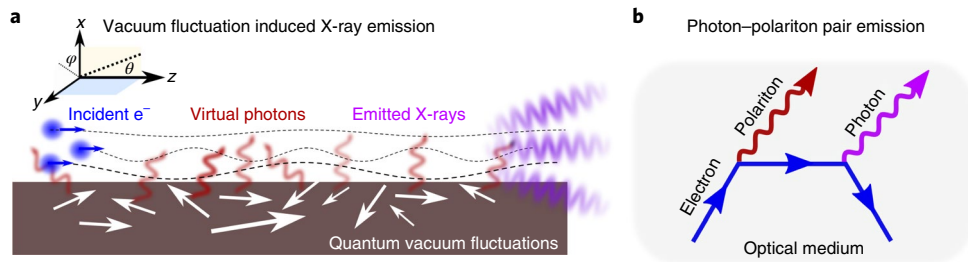
Fig. 1 | Light emission induced by nanophotonic vacuum fluctuations and spontaneous emission of a photon–polariton pair. a, Schematic illustrating a beam of electrons travelling in the near field of a nanophotonic structure. The vacuum fields lead to random modulations of the trajectory with a non-zero variance. These modulations lead in turn to a Doppler shift of the vacuum fluctuations into a higher frequency in the electron's rest frame, resulting in photon output at even higher frequencies. The ratio of the output photon frequency to polariton frequency scales as $\left(\frac{E}{mc^2}\right)^2$, where E is the energy of the electron, resulting in enormous frequency up-conversion factors for relativistic electrons. **b**, The complementary description in QED: a second-order two-quantum (spontaneous) emission process involving a mode of the structure (denoted polariton) and a high-energy photon.

X-rays (for few-megaelectronvolt electrons attainable with a table-top radiofrequency gun) and gamma rays (with further electron acceleration). Despite the output being at such high frequencies, the spatial and temporal properties of the emitted photons can be tailored by controlling the material permittivity at IR frequencies. We illustrate these concepts in tunable nanophotonic materials of current interest such as graphene, a dynamically tunable plasmonic material known to support highly confined and low-loss plasmons at infrared frequencies[38–42]. Our results may be enabling concepts for novel passive and compact sources of tunable radiation from nanometre to femtometre wavelengths. Our results also suggest a novel 'nonlinearity' mediated by relativistic electrons that couples low-frequency (IR or optical) fields to high-frequency (UV, X-ray or gamma ray) fields despite the well-known lack of electromagnetic response at such high frequencies. Our findings may also yield a new way to study the quantized electromagnetic vacuum: through high-frequency light emitted into the far field by a relativistic probe.

Spontaneous emission of a photon–polariton pair

Consider a beam of electrons travelling over a photonic structure that permits strong coupling of light and material polarization (Fig. 1a). Examples of such a structure include all-dielectric nanostructures or materials with resonances associated with plasmon-, phonon-, exciton- or magnon-polaritons. For brevity, we will refer to any mode arising from non-trivial optical response as a polariton mode, even those in all-dielectric structures, as the non-trivial optical response is concomitant with strong coupling between light and material polarization. The electrons are affected by electromagnetic field fluctuations that arise from the quantum fluctuations of polarization currents inside the material. Although this fluctuating field has zero mean, it has a non-zero variance that leads to the possibility of far-field photon emission by the electron through spontaneous emission. In this spontaneous emission process, a far-field photon and a photonic mode of the nanostructure (a polariton mode) are simultaneously emitted. We henceforth refer to this two-quantum emission as a photon–polariton pair emission. The probability of two-quantum emission processes scales as the square of the fine-structure constant ($\alpha \approx 1/137$), which led to a long delay between prediction and the first direct observation in the specific case of two-photon emission from atoms[43,44]. However, two-quantum emission can be strongly enhanced by nearby polaritonic media in atomic or low-energy emitters based on bound charges, making these two-polariton emission processes strong or potentially even dominant[45–48] over single-photon decay channels. Two-photon emission by free electrons was suggested by luminaries such as Ilya Frank in his 1958 Nobel lecture on the Cherenkov effect[49], and was considered as a second-order Cherenkov effect[50,51].

Figure 1 summarizes the discussion above by illustrating the two complementary paradigms that can be used to explain the phenomena we study here. The first is the fluctuational electrodynamics paradigm (Fig. 1a) where a free electron radiates as a result of interactions with fluctuating fields in a nanophotonic vacuum (derived and applied in Supplementary Sections 3 and 4). The second is the QED paradigm (Fig. 1b), which describes the radiation as part of a second-order quantum process in which a relativistic electron spontaneously emits one photon and one polariton (derived in Supplementary Section 5 via both scalar and Dirac QED, which agree well with electron energies below 1 GeV). We show that the QED approach leads to the same results. We encourage the reader to see the Methods for a summary of the essentials of the derivation of the spectrum and intensity of photon–polariton pair emission from fluctuational electrodynamics.

Impact of polariton confinement on the emission

We find that in photon–polariton pair emission by an electron with speed $v = c\beta$ moving along direction $\hat{\mathbf{v}}$, where c is the speed of light, the photon and polariton are kinematically related (see Supplementary Section 4). In particular, a photon emitted of frequency ω' along direction $\hat{\mathbf{n}}$ is kinematically related to a polariton emitted of frequency ω_q in direction $\hat{\mathbf{q}}$ by

$$\omega' = \omega_q \frac{\beta n(\omega_q)\cos\theta_q - 1}{1 - \beta\cos\theta} \tag{1}$$

where $n(\omega_q) = qc/\omega_q$ is the effective mode index of the polariton (with q the magnitude of the polariton wavevector), $\cos\theta_q = \hat{\mathbf{q}} \cdot \hat{\mathbf{v}}$, and $\cos\theta = \hat{\mathbf{n}} \cdot \hat{\mathbf{v}}$. Note that the frequency is independent of the azimuthal angle φ of the photon as defined in Fig. 1a. Equation (1) reveals two ways by which the photon frequency can be greatly enhanced. The first way is by minimizing the denominator, which is achieved by using high-energy electrons and collecting photons emitted in the direction of electron motion ($\theta = 0$), as can be seen by the fact that $(1 - \beta\cos\theta)^{-1} \approx 2\gamma^2$ when $\theta = 0$ and $\beta \approx 1$. The second way is by making use of an optical medium that supports polariton modes of simultaneously high wavevector and high effective mode indices.

The numerator in equation (1) reveals a fundamental difference between the process studied here and a potential process in which a photon is emitted and a polariton is absorbed. In this latter case, the numerator of equation (1) would change to $vq_{\parallel} + \omega$ (with $q_{\parallel} = \mathbf{q} \cdot \hat{\mathbf{v}}$, see Supplementary Section 4), implying that strong enhancement of radiated frequency can occur even when $q_{\parallel} = 0$. For a photon–polariton
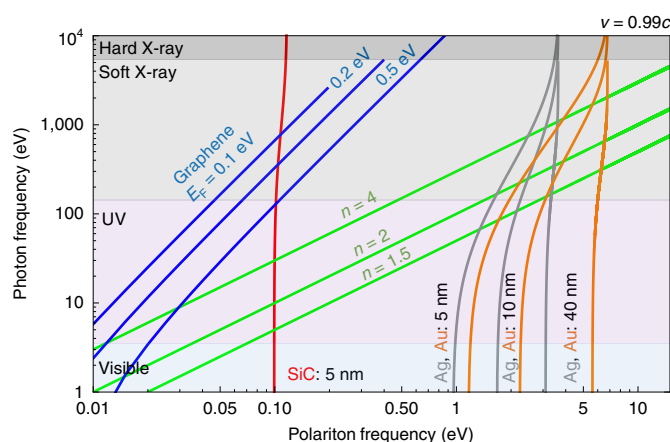
Fig. 2 | Influence of optical materials on the photon emission spectrum in photon–polariton pair emission. Radiated photon frequency of equation (1) for photons emitted along $\theta = 0$, and polaritons emitted along $\theta_q = 0$ (both emitted forwards). The photon frequency is shown as a function of polariton frequencies for plasmons in (Drude) gold and silver with different thicknesses, (Drude) graphene with different doping levels, and phonon polaritons in silicon carbide. Also shown are contours corresponding to a constant index of refraction $n = 1.5$, 2 and 4. Despite the very different frequencies of plasmons in graphene, phonon polaritons in silicon carbide, and plasmons in silver and gold, all of these materials are capable of being used for generation of hard X-ray photons.

pair emission process, emission is kinematically forbidden for $q_{\parallel} < \omega/v$. This implies that high-frequency modes are not necessarily associated with the generation of high-frequency photons in photon–polariton pair emission. Instead, high mode indices are necessary.

The importance of high mode indices in generating high-frequency photons is summarized in Fig. 2, where we plot the relationship between the emitted photon frequency and the emitted polariton frequency for different optical materials, in the scenario where both the polariton and photon are emitted in the forward direction by an electron moving at a speed of $0.99c$. We consider plasmonic thin films of gold and silver of varying thickness; two-dimensional plasmonic materials such as graphene, with varying levels of doping; and thin films of phonon polaritonic materials such as silicon carbide. As can be seen from Fig. 2, despite the widely different frequencies of the emitted polaritons in these widely different materials, the emitted photons can be at hard X-ray frequencies (frequencies in excess of 5 keV). To summarize this figure: high mode momentum (provided it comes with a high mode index) leads to high-frequency photons.

To highlight further the interplay of electron velocity and polariton mode index on the output photon frequency, we present another example. For graphene, with Fermi energy 0.5 eV, the forward emission of a plasmon of 0.5 eV frequency will be concomitant with the forward emission of a photon of frequency 110 eV for an electron with velocity $0.7c$ (as from a transmission electron microscope), a photon of frequency 6.7 keV for an electron with velocity $0.995c$ (as from a radiofrequency gun), and a photon of frequency 675 keV for an electron with velocity $0.99995c$ (from a linear accelerator). Meanwhile, if the plasmon is replaced by a polariton of frequency 100 eV but a mode index of 1.01, then for an electron of velocity $0.7c$, it is kinematically forbidden to emit a photon. For an electron of velocity $0.995c$, the outgoing photon has a frequency of 0.099 keV, and for an electron of velocity $0.99995c$, the outgoing photon has a frequency of 20 keV.

Strong high-frequency radiation from vacuum fluctuations
Having discussed the kinematics of photon–polariton pair emission, we now move to analyse the angular and frequency correlations of

the emitted photon–polariton pairs, as well as the overall strength of the process. To make the discussion concrete, we consider this process when the emitted polariton is a plasmon in graphene, a dynamically tunable plasmonic material known to support plasmons that simultaneously have high mode index and low-enough losses to be well-defined excitations. Graphene is a very attractive platform for realizing the effect we describe in this Article. Besides having highly confined plasmons that propagate for reasonably long distances, it is also tunable, has a very high surface-to-bulk ratio and can be produced in suspended form, allowing the minimization of background effects. That said, we show (in Supplementary Fig. 4) that other materials, such as thin films of gold, can give effects of a similar magnitude, as could be anticipated from the utility of conventional plasmonic materials in fields such as near-field radiative heat transfer. The low damping also could allow the intriguing possibility that the emitted polariton could re-interact with the electron beam, leading to feedback and radiation enhancement.

In particular, we consider the photon–polariton pair emission process for a fast electron moving parallel to a sheet of doped graphene, a distance x_0 away from the surface of the graphene. We consider the graphene to be free-standing, although the conclusions of Figs. 3 and 4 are not qualitatively changed when a transparent substrate is introduced. Note that for simple exposition, we model graphene via a Drude model with an infinite Drude relaxation time. A realistic Drude relaxation time has little effect on the emitted power (see Supplementary Fig. 2). We also consider the influence of interband transitions modelled through the local and non-local conductivity derived from the random-phase approximation. The output power in those cases remains similar to the Drude case.

Spectral and angular correlations between the emitted photon and polariton. In photon–polariton pair emission, the fast electron spontaneously emits a photon and a plasmon-polariton, whose spatial and spectral distributions are shown in Fig. 3. In Fig. 3a (upper semicircle), we show the radiated photon energy per unit time (photon power) per unit plasmon frequency, plasmon angle and photon angle, with fixed photon angle ($\theta = 0$). The electron is taken to have a velocity of $0.99c$. Integrating over these variables gives the total emitted power. The (polar) plot shows this differential power as a function of the plasmon frequency ω_q (radial direction) and plasmon angle θ_q (angular direction). We represent the spectrum this way to show how the emission intensity depends on the kinematical properties of the individual photon–plasmon pairs.

Figure 3a highlights two main features of photon–polariton pair emission. First, the plasmons are preferentially emitted into the graphene sheet in a direction perpendicular to the direction of electron motion. This results from the polarization of a highly confined plasmon, which is half in the direction of plasmon propagation and half perpendicular to the graphene sheet. For a plasmon emitted parallel to the direction of electron motion, half of the plasmon polarization is in the direction of electron motion, which for relativistic electrons has very little impact on the modulation of the electron trajectory. This component is thus incapable of modulating the electron trajectory and makes little contribution to the emitted power. Meanwhile, for a plasmon emitted perpendicular to the electron motion, every component of the polarization is transverse to the electron's unperturbed trajectory, and thus effectively modulates the trajectory. The second feature is that very little photon emission corresponds to emission of plasmons of frequency less than 0.25 eV or more than 1 eV. The lack of low-frequency plasmons results from the low density of states of the plasmons at low frequency. The lack of high-frequency plasmons results from the fact that their evanescent tails become substantially smaller than x_0, rendering the electron insensitive to those plasmon modes. The lower semicircle shows the photon frequencies that correspond to a particular plasmon angle and plasmon frequency. We see clearly that the emission of plasmons
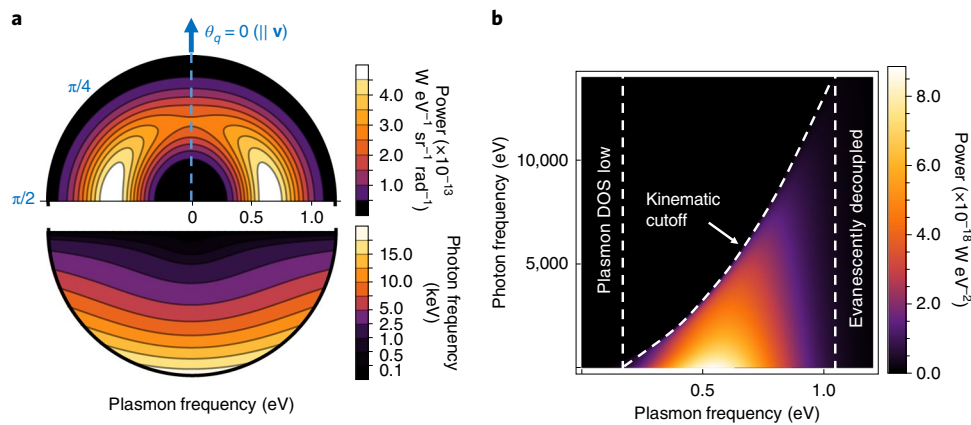
Fig. 3 | Correlations between emitted infrared polaritons and emitted X-ray photons in photon–polariton pair emission. a, Top: polar plot of emitted photon power in photon–polariton pair emission, when the polariton is a plasmon in doped graphene. The power is per unit plasmon frequency, per unit plasmon angle and per unit photon angle for forward photon emission $\theta = 0$, plotted as a function of plasmon frequency (radial direction) and plasmon angle (angular direction). A preference exists for plasmons emitted perpendicular to the direction of electron motion due to polarization effects. Bottom: corresponding frequencies for the forward-emitted photon as a function of plasmon energy and angle. **b**, Emitted photon power per unit photon frequency and plasmon frequency, which show a clear correlation between plasmon and photon frequencies. The photon emission is synchrotron-like, extending from UV to X-ray frequencies, having maximum contribution from plasmon frequencies where the local density of states (DOS) is highest. The electron is taken to have a velocity of 0.99c, and travels a distance $x_0 = 5$ nm away from the surface of the graphene sheet, which is doped to a Fermi energy of 0.5 eV.

at perpendicular angles corresponds to low photon energies, which follows from equation (1). As a result of the continuum of plasmon angles and energies in the sheet geometry, the photon emission is quite broadband, spanning from the soft UV to hard X-ray frequencies, similar to synchrotron light.

In Fig. 3b, we elaborate further on the correlated nature of the photon–polariton pair emission by showing the photon power emitted per unit plasmon frequency and photon frequency, which represents the spectral intensity of plasmon–photon correlations. Integrating over these variables gives the total emitted power. From Fig. 3b, we notice first that the emission of a plasmon with frequencies between 0 and 1 eV is correlated with photon emission from 0 to nearly 10 keV. Higher frequency photons are correlated with higher frequency plasmons, as expected from equation (1). For a photon of any frequency, it is most correlated with a plasmon that has a substantial density of states, but is also not evanescently decoupled from the electron, which in the case of Fig. 3b occurs for plasmons of frequency around 0.5 eV.

For any plasmon frequency, photons have a slight preference to be emitted at lower frequencies (most of the emission is nevertheless in between 1 and 5 keV). This can be understood from the fact that plasmons are preferentially emitted near $\theta_q = \pi/2$, as shown in Fig. 3a. Supplementary Figure 1 shows the same overall phenomena as in Fig. 3 but for different Fermi energy in graphene (and different x_0), which results in a different plasmon dispersion and thus a change in the angular and spectral properties of the emission. This shows that the emitted X-rays can be tuned by changing the modal properties of photons in the IR, whether it be the dispersion relation or polarization properties.

Total radiated power in photon–polariton pair emission. We now evaluate the total power emitted in photon–polariton pair emission. A key result is the total emitted power integrated over all photon and plasmon properties, plotted in Fig. 4a as a function of electron energy and distance between the electron and the surface. The emitted power increases sharply with increasing electron energy (as γ^2, with γ being the ratio between the electron energy and its rest mass energy) and decreasing distance to the surface (as $x_0^{-7/2}$). This $x_0^{-7/2}$ dependence arises from the Drude model in the quasi-electrostatic limit, and breaks down for

distances on the order below 1 nm, when effects of quantum non-locality become strong, and above about a micrometre, where retardation becomes significant.

As a numerical example, consider a scenario in which a 500 MeV electron travels within 5 nm from the surface of graphene doped to Fermi energy 0.5 eV. A typical value of power emitted in the photon component of photon–polariton pair emission in this distance range is about 1.3 nW (for example, for $x_0 = 3$ nm). As a point of comparison, we also consider a scenario in which a 500 MeV electron emits synchrotron radiation as a result of travelling in a circular orbit in a 1 T magnetic field. The power emitted through synchrotron radiation is about 15 nW. The closeness of these two powers is a surprising observation given that in the former scenario, vacuum fluctuations drive the radiation, whereas in the latter scenario, a strong applied magnetic field drives the radiation. Although we referred to a specific electron energy, this was solely for concreteness, as our finding applies at any electron energy, since the emitted powers of photon–polariton pair emission and synchrotron radiation both scale in the same manner with electron energy (as γ^2). We encourage the reader to see Supplementary Section 2 to see more details about the characteristic photon emission rates, methods to scale up the output brightness and comparison to other miniaturized light sources. Regarding other miniaturized light sources, particularly based on strongly pumping a near-field of a photonic structure, we found that the photon–polariton pair emission, although passive, can lead to as much integrated power as in the situation in which the electron radiates as a result of scattering from an externally pumped near-field containing thousands of quanta.

We now quantitatively explain why the magnitude of this vacuum-induced emission process can be comparable to processes that rely on substantial external driving fields, such as magnetic fields of 1 T. Our explanation is based on an analytical formula for total emitted power P that we obtain in the limit where photon–polariton pair emission is dominated by highly confined polariton modes. In this limit, the power is given by:

$$P = \frac{e^4 \gamma^2 (4 - \beta^2)}{24\pi\epsilon_0 m^2 c^3} \langle 0|\mathbf{E}^2|0\rangle \qquad (2)$$
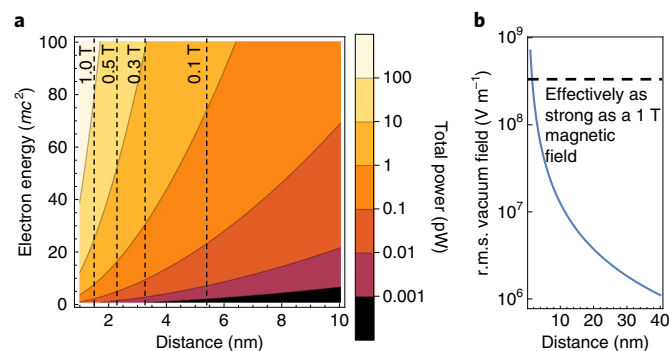
Fig. 4 | Total emitted power due to nanoplasmonic vacuum fluctuations. a, Total photon power as a function of electron energy (in units of the rest mass energy) and distance to a graphene sheet. Vertical dashed lines correspond to synchrotron radiation power for different values of a hypothetical driving magnetic field. **b**, Dependence of the r.m.s. of the graphene-plasmon contribution to the quantized electric field as a function of the distance to the surface of a sheet of graphene doped to a Fermi energy of 0.5 eV.

where $\langle 0|\mathbf{E}^2|0\rangle$ is the expectation value of the quantized electric field associated with plasmonic zero-point fluctuations. Note that we calculate the fluctuations resulting from the medium and remove the contribution of free-space fluctuations to the squared electric field, as they give zero contribution due to energy–momentum conservation. A detailed derivation of this expression is shown in Supplementary Section 5. Equation (2) is simply the Larmor formula from classical electrodynamics for a charged particle of acceleration a given in this case by $a = \frac{eE_{r.m.s.}}{m\gamma}$, with the root-mean squared (r.m.s) electric field defined by $E_{r.m.s.} \equiv \sqrt{\langle 0|\mathbf{E}^2|0\rangle}$. To see how this explains the high radiated power in photon–polariton pair emission, consider Fig. 4b, which shows the r.m.s. plasmonic field as a function of distance from the graphene surface. The magnitude of the r.m.s. fluctuations 5 nm from the surface is about 50 MV m⁻¹, which induces electron acceleration magnitudes that one expects to find for an electron in a magnetic field of 0.2 T in a synchrotron. Similarly, the magnitude of the quantum r.m.s. field 1 nm away from the surface is about 300 MV m⁻¹, which induces electron acceleration magnitudes that one expects to find for an electron in a magnetic field of 1 T. More generally, the power radiated by an electron undergoing synchrotron radiation in a uniform magnetic field B is $P = \frac{e^4\gamma^2 B^2}{6\pi\epsilon_0 m^2 c}$, revealing that the power radiated from photon–polariton pair emission (equation (2)) is comparable with that from synchrotron radiation when $\sqrt{\langle \mathbf{E}^2 \rangle}$ and cB in the respective processes are comparable. These examples emphasize the strong fields that arise from vacuum fluctuations, and explain the high emitted power we find in Fig. 4a. To conclude this section, we note that equation (2) also allows us to immediately understand the $x_0^{7/2}$ dependence of the power mentioned earlier. In particular, the expectation value of the squared electric field operator associated with Drude plasmons is given by $\int \frac{dq}{2\pi} \frac{\hbar\omega_q q^2}{2\epsilon_0} e^{-2qx_0} \sim x_0^{-7/2}$ for $\omega_q \sim \sqrt{q}$.

Discussion

One potential method of experimentally demonstrating photon–polariton pair emission would be to send a beam of electrons close to a nanostructure, and at grazing incidence, in a set-up capable of detecting very high-frequency radiation (for example, with energy dispersive X-ray detectors[52]), making sure to account for competing bremsstrahlung by electrons that penetrate the material. Yet another meaningful experimental demonstration would use time-synchronized measurements of coincidences to measure spatiotemporal

correlations between the X-ray photon and the emitted polariton. The relevant set-up depends on the energy scale. For example, electrons could be accelerated to 200 keV kinetic energy in an electron microscope. MeV electron energies could be achieved by a radio-frequency gun or with potential advances in dielectric laser acceleration[53]. GeV electron energies could be achieved with a linear accelerator or potentially with plasma wakefield acceleration[54].

An alternative experimental demonstration could involve the detection—through electron energy-loss spectroscopy (EELS)—of anomalously high energy losses in the electrons that pass a small distance away from the surface at grazing incidence. This would require one to be able to differentiate X-ray losses from core loss transitions in the materials near the surface, which is possible due to the tunability of the photon spectrum (because the EELS peaks from photon–polariton pair emission shift by varying acceleration voltage or nanophotonic geometry as per equation (1)). In Supplementary Section 2, we briefly discuss methods to minimize background effects that also produce X-rays associated with electrons colliding into the sample.

The concept developed here applies to, and is enriched by, the consideration of alternative materials and structures. Examples include thin films and quasi-two-dimensional systems ('transdimensional' systems[55]) of plasmonic materials such as gold, silver and titanium nitride[56], as well as more general polaritonic materials and metasurfaces. One can consider optimizing various radiation characteristics through optimizing the nanophotonic structure. For example, a structure that could make the radiation more monochromatic would enhance the spectral density, quality and brightness of the X-ray source. Better monochromaticity could potentially be achieved by structuring a material into a nanograting, such that the X-ray frequency is selected by reciprocal lattice vectors of the grating. The goal of designing radiation sources through our formalism will benefit from the great computational strides that have been made in calculating fluctuation spectra near complicated arrangements and geometries of optical media[25,27,57]. The framework advanced here can also be extended to other charge distributions using results from classical electrodynamics to accommodate radiation from more complicated systems of charges such as moving dipoles or bunched electrons (including periodically bunched electrons, which are typical in free-electron laser settings). Beyond the possibilities of applying this concept to compact and tunable sources of high-frequency light, the ability to control spontaneous free-electron emission at arbitrarily high frequencies may also ultimately lead to the ability to create synthetic active nonlinearities at X-ray[58–60] and perhaps gamma-ray frequencies controlled by now accessible nanopatterning of photonic systems.

Online content

Any methods, additional references, Nature Research reporting summaries, source data, statements of code and data availability and associated accession codes are available at https://doi.org/10.1038/s41567-019-0672-8.

References

1. Dirac, P. A. The quantum theory of the emission and absorption of radiation. *Proc. R. Soc. Lond. A* **114**, 243–265 (1927).
2. Lamb, W. E. Jr & Retherford, R. C. Fine structure of the hydrogen atom by a microwave method. *Phys. Rev.* **72**, 241–243 (1947).
3. Lifshitz, E. The theory of molecular attractive forces between solids. *Sov. Phys. JETP* **2**, 73–83 (1956).
4. Sandoghdar, V., Sukenik, C., Hinds, E. & Haroche, S. Direct measurement of the van der Waals interaction between an atom and its images in a micron-sized cavity. *Phys. Rev. Lett.* **68**, 3432–3435 (1992).
5. Chan, H. B., Aksyuk, V. A., Kleiman, R. N., Bishop, D. J. & Capasso, F. Quantum mechanical actuation of microelectromechanical systems by the Casimir force. *Science* **291**, 1941–1944 (2001).

6. Pendry, J. Shearing the vacuum-quantum friction. *J. Phys. Condens. Matter* **9**, 10301–10320 (1997).
7. Johansson, J. R., Johansson, G., Wilson, C. & Nori, F. Dynamical Casimir effect in a superconducting coplanar waveguide. *Phys. Rev. Lett.* **103**, 147003 (2009).
8. Nation, P., Johansson, J., Blencowe, M. & Nori, F. Colloquium: Stimulating uncertainty: amplifying the quantum vacuum with superconducting circuits. *Rev. Mod. Phys.* **84**, 1–24 (2012).
9. Fulling, S. A. Nonuniqueness of canonical field quantization in Riemannian space-time. *Phys. Rev. D* **7**, 2850–2862 (1973).
10. Davies, P. C. Scalar production in Schwarzschild and Rindler metrics. *J. Phys. A* **8**, 609–616 (1975).
11. Unruh, W. G. Notes on black-hole evaporation. *Phys. Rev. D* **14**, 870–892 (1976).
12. Joannopoulos, J. D., Johnson, S. G., Winn, J. N. & Meade, R. D. *Photonic Crystals: Molding the Flow of Light* (Princeton Univ. Press, 2011).
13. Basov, D., Fogler, M. & de Abajo, F. G. Polaritons in van der Waals materials. *Science* **354**, aag1992 (2016).
14. Low, T. et al. Polaritons in layered two-dimensional materials. *Nat. Mater.* **16**, 182–194 (2017).
15. Purcell, E. M. Spontaneous emission probabilities at radio frequencies. *Phys. Rev.* **69**, 681 (1946).
16. Kleppner, D. Inhibited spontaneous emission. *Phys. Rev. Lett.* **47**, 233–236 (1981).
17. Yablonovitch, E. Inhibited spontaneous emission in solid-state physics and electronics. *Phys. Rev. Lett.* **58**, 2059–2062 (1987).
18. Luo, C., Ibanescu, M., Johnson, S. G. & Joannopoulos, J. Cerenkov radiation in photonic crystals. *Science* **299**, 368–371 (2003).
19. De Abajo, F. G. Optical excitations in electron microscopy. *Rev. Mod. Phys.* **82**, 209–275 (2010).
20. Sapienza, R. et al. Deep-subwavelength imaging of the modal dispersion of light. *Nat. Mater.* **11**, 781–787 (2012).
21. Yang, Y. et al. Maximal spontaneous photon emission and energy loss from free electrons. *Nat. Phys.* **14**, 894–899 (2018).
22. Rivera, N., Wong, L. J., Soljačić, M. & Kaminer, I. Ultrafast multiharmonic plasmon generation by optically dressed electrons. *Phys. Rev. Lett.* **122**, 053901 (2019).
23. Pendry, J. Radiative exchange of heat between nanostructures. *J. Phys. Condens. Matter* **11**, 6621–6633 (1999).
24. Volokitin, A. & Persson, B. N. Near-field radiative heat transfer and noncontact friction. *Rev. Mod. Phys.* **79**, 1291–1329 (2007).
25. Reid, M. H., Rodriguez, A. W., White, J. & Johnson, S. G. Efficient computation of Casimir interactions between arbitrary 3D objects. *Phys. Rev. Lett.* **103**, 040401 (2009).
26. Otey, C. R. et al. Thermal rectification through vacuum. *Phys. Rev. Lett.* **104**, 154301 (2010).
27. Rodriguez, A. W., Capasso, F. & Johnson, S. G. The Casimir effect in microstructured geometries. *Nat. Photon.* **5**, 211–221 (2011).
28. Shen, S., Narayanaswamy, A. & Chen, G. Surface phonon polaritons mediated energy transfer between nanoscale gaps. *Nano Lett.* **9**, 2909–2913 (2009).
29. Rousseau, E. et al. Radiative heat transfer at the nanoscale. *Nat. Photon.* **3**, 514–517 (2009).
30. Kim, K. et al. Radiative heat transfer in the extreme near field. *Nature* **528**, 387–391 (2015).
31. Jackson, J. D. *Classical Electrodynamics* (Wiley, 1999).
32. Friedman, A., Gover, A., Kurizki, G., Ruschin, S. & Yariv, A. Spontaneous and stimulated emission from quasifree electrons. *Rev. Mod. Phys.* **60**, 471–535 (1988).
33. Ginsburg, V. *Applications of Electrodynamics in Theoretical Physics and Astrophysics* (Routledge, 1989).
34. Pellegrini, C., Marinelli, A. & Reiche, S. The physics of X-ray free-electron lasers. *Rev. Mod. Phys.* **88**, 015006 (2016).
35. Wong, L. J., Kaminer, I., Ilic, O., Joannopoulos, J. D. & Soljačić, M. Towards graphene plasmon-based free-electron infrared to X-ray sources. *Nat. Photon.* **10**, 46–52 (2016).
36. Rosolen, G. et al. Metasurface-based multi-harmonic free-electron light source. *Light Sci. Appl.* **7**, 64 (2018).
37. Feranchuk, I. & Ivashin, A. Theoretical investigation of the parametric X-ray features. *J. Phys.* **46**, 1981–1986 (1985).
38. Jablan, M., Buljan, H. & Soljačić, M. Plasmonics in graphene at infrared frequencies. *Phys. Rev. B* **80**, 245435 (2009).
39. Chen, J. et al. Optical nano-imaging of gate-tunable graphene plasmons. *Nature* **487**, 77–81 (2012).
40. Fei, Z. et al. Gate-tuning of graphene plasmons revealed by infrared nano-imaging. *Nature* **487**, 82–85 (2012).
41. Iranzo, D. A. et al. Probing the ultimate plasmon confinement limits with a van der Waals heterostructure. *Science* **360**, 291–295 (2018).
42. Ni, G. et al. Fundamental limits to graphene plasmonics. *Nature* **557**, 530–533 (2018).
43. Göppert-Mayer, M. Über elementarakte mit zwei quantensprüngen. *Ann. Phys.* **401**, 273–294 (1931).
44. Cesar, C. L. et al. Two-photon spectroscopy of trapped atomic hydrogen. *Phys. Rev. Lett.* **77**, 255–258 (1996).
45. Hayat, A., Ginzburg, P. & Orenstein, M. Observation of two-photon emission from semiconductors. *Nat. Photon.* **2**, 238–241 (2008).
46. Nevet, A. et al. Plasmonic nanoantennas for broad-band enhancement of two-photon emission from semiconductors. *Nano Lett.* **10**, 1848–1852 (2010).
47. Rivera, N., Kaminer, I., Zhen, B., Joannopoulos, J. D. & Soljačić, M. Shrinking light to allow forbidden transitions on the atomic scale. *Science* **353**, 263–269 (2016).
48. Rivera, N., Rosolen, G., Joannopoulos, J. D., Kaminer, I. & Soljačić, M. Making two-photon processes dominate one-photon processes using mid-IR phonon polaritons. *Proc. Natl. Acad. Sci. USA* **114**, 13607–13612 (2017).
49. Frank, I. Optics of light sources moving in refractive media. *Science* **131**, 702–712 (1960).
50. Batygin, V. On the possibility of hard Vavilov–Cerenkov radiation. *Sov. Phys. JETP* **21**, 179–180 (1965).
51. Batygin, V. & Kuz'menko, K. Quantum theory of Vavilov–Cerenkov radiation by an electron traveling in vacuum parallel to a dielectric surface. *Sov. Phys. JETP* **68**, 437–440 (1975).
52. Goldstein, J. I. et al. *Scanning Electron Microscopy and X-ray Microanalysis* (Springer, 2017).
53. England, R. J. et al. Dielectric laser accelerators. *Rev. Mod. Phys.* **86**, 1337–1389 (2014).
54. Blumenfeld, I. et al. Energy doubling of 42 GeV electrons in a metre-scale plasma wakefield accelerator. *Nature* **445**, 741–744 (2007).
55. Boltasseva, A. & Shalaev, V. M. Transdimensional photonics. *ACS Photon.* **6**, 1–3 (2019).
56. Naik, G. V. et al. Titanium nitride as a plasmonic material for visible and near-infrared wavelengths. *Opt. Mater. Express* **2**, 478–489 (2012).
57. Rodriguez, A. W., Reid, M. H. & Johnson, S. G. Fluctuating-surface-current formulation of radiative heat transfer for arbitrary geometries. *Phys. Rev. B* **86**, 220302 (2012).
58. Freund, I. & Levine, B. Parametric conversion of X-rays. *Phys. Rev. Lett.* **23**, 854–857 (1969).
59. Eisenberger, P. & McCall, S. X-ray parametric conversion. *Phys. Rev. Lett.* **26**, 684–688 (1971).
60. Glover, T. et al. X-ray and optical wave mixing. *Nature* **488**, 603–608 (2012).

Author contributions
N.R. led the work with substantial input from all other authors.

Competing interests
The authors declare no competing interests.

Additional information
Supplementary information is available for this paper at https://doi.org/10.1038/s41567-019-0672-8.

Correspondence and requests for materials should be addressed to N.R. or I.K.

Peer review information *Nature Physics* thanks Frank Koppens and Kimball Milton for their contribution to the peer review of this work.

Reprints and permissions information is available at www.nature.com/reprints.

Publisher's note Springer Nature remains neutral with regard to jurisdictional claims in published maps and institutional affiliations.

Methods

In this section we present an overview of the fluctuational electrodynamics formalism used to calculate the spectrum of photon–polariton pair emission. Further details are provided in Supplementary Sections 3 and 4. We emphasize that this formalism, for parameters considered in the main text, gives precisely the same result as a calculation based on the direct calculation of the emission based on second-order time-dependent perturbation theory (shown in Supplementary Section 5).

From the point of view of fluctuational electrodynamics, it is sufficient here to consider a classical electron travelling initially in a straight line with velocity $\mathbf{v} = c\boldsymbol{\beta}$ and position $\mathbf{r}(t) = \mathbf{r}_0 + \mathbf{v}t$, with $\mathbf{r}_0$ being the position taken at an arbitrarily chosen origin of time $t = 0$. In the presence of an external modulating electric field, this electron will experience an acceleration that leads to subsequent radiation, as prescribed by the Liénard–Wiechert potentials, the essential aspects of which are summarized in the Supplementary Information. The radiated energy is quadratic in the modulating field. In the spirit of the discussion of Fig. 1a, we identify the modulating field with that associated with the quantum fluctuations of the nanophotonic vacuum at thermal equilibrium. The average power radiated by the electron is governed by the correlation function between different components of the fluctuating electric field at different positions and different times. This correlation function is $\langle E_i(\mathbf{r}, t)E_j(\mathbf{r}', t')\rangle$, where $\mathbf{r}$ and $\mathbf{r}'$ are different points in space, t and t' are different points in time, E_i is the ith component of the quantized electric field operator, and $\langle\rangle$ denotes an ensemble average assuming thermal equilibrium. From the quantum theory of the macroscopic electromagnetic field in an arbitrary dielectric medium, $\langle E_i(\mathbf{r}, t)E_j(\mathbf{r}', t')\rangle$, at zero temperature, is given by[61–63]:

$$\frac{\hbar}{\pi\epsilon_0 c^2}\int_0^\infty d\omega\ \omega^2\mathrm{Im}\ G_{ij}(\mathbf{r}(t), \mathbf{r}(t'), \omega)e^{-i\omega(t-t')} \tag{3}$$

with ϵ_0 the permittivity of free space, and $\hbar$ the reduced Planck constant. The non-zero temperature generalization is presented in the Supplementary Information. In this equation, the integration variable ω can be interpreted as the angular frequency of a polariton in the nanophotonic structure. In practice, the integral in equation (3) is well-approximated by restricting the range of integration to the set of frequencies where the local density of states of the polaritons are high. G_{ij} is the dyadic Green's function of the nanophotonic structure and is dependent on material resonances and material geometry.

To find the energy radiated per unit photon frequency ω' and photon solid angle Ω into the far-field, $dU/d\omega'd\Omega$, we take the an ensemble average of the radiated power over realizations of the modulating field, thus plugging in equation (3) for the ensemble averaged modulating field (a detailed derivation is given in Supplementary Section 3). The result of this fluctuational electrodynamics calculation, at zero temperature, is:

$$\frac{dU}{d\omega'd\Omega} = \frac{e^4\hbar}{16\pi^4\epsilon_0^2 m^2 c^5\gamma^2(1-\beta\cos\theta)^4}$$
$$\times\int_{-\infty}^\infty dtdt'\int_0^\infty d\omega\ \omega^2\mathrm{Im}\,[e^{-i(\omega+\omega')(1-\beta\cos\theta)(t-t')}\mathrm{tr}\,[\mathbf{T}\mathbf{G}(\mathbf{r}(t), \mathbf{r}(t'), \omega)\mathbf{T}^\mathrm{T}]] \tag{4}$$

where $\gamma = (1-\beta^2)^{-1/2}$ is the electron Lorentz factor, θ is the angle of the emitted photon with respect to the direction of electron motion, and t and t' are times that are integrated over the electron's unperturbed linear trajectory. Additionally, we have defined the matrix T, whose components $T_{ij} \equiv (\beta\cos\theta-1)\delta_{ij} - (\hat{n}_i - \beta_i)\hat{n}_j$, with δ_{ij} a Kronecker delta, $\hat{\mathbf{n}}$ a unit vector along the direction of photon emission, and $\mathbf{E}_\gamma = \left(\mathbf{E}_\perp, \frac{E_\parallel}{\gamma^2}\right)$ where $\perp$ ($\parallel$) denote directions perpendicular (parallel) to $\mathbf{v}$. The only assumptions made in writing equation (4) are that the deviations of the electron motion from a straight-line trajectory are fairly small, and that the fluctuating fields are quasi-electrostatic in nature, meaning that effects of the magnetic fields are negligible compared to those of the electric fields, which holds for highly confined near fields associated with polaritons in dielectrics and conductors. We note that the assumption of zero temperature is well-respected even at room temperature, as for the IR polariton frequencies we consider here, $\frac{kT}{\hbar\omega} \ll 1$, with k being Boltzmann's constant. However, at higher temperatures, the emission will be enhanced due to contributions from thermal near-field fluctuations. Equation (4) is the main formal result of this work, and it is applied in the main text. We comment that in the fluctuational electrodynamics paradigm, the effect we describe can be phrased as follows: fluctuating polarization currents in a medium lead to fluctuating acceleration and thus fluctuating dipole moments of an electron, leading to subsequent high-frequency radiation, due to the relativistic speed of the electron. In these terms, the physics is like that of the general Casimir–Polder effect (which has the van der Waals force as its near-field limit), where vacuum fluctuations lead to a force on a bound electron in an atom or molecule. Unlike other often considered Casimir phenomena, this vacuum force acts on a relativistic free electron and oscillates it, leading to the radiation emission.

Data availability

The data represented in Figs. 2–4 are available as Supplementary information files. All other data that support the plots within this paper and other findings of this study are available from the corresponding author on reasonable request.

References

61. Rytov, S., Kravtsov, Y. A. & Tatarskii, V. *Principles of Statistical Radiophysics. 3. Elements of Random Fields* (Springer, 1989).
62. Scheel, S. & Buhmann, S. Macroscopic quantum electrodynamics-concepts and applications. *Acta Phys. Slov.* **58**, 675–809 (2008).
63. Lifshitz, E. M. & Pitaevskii, L. P. *Statistical Physics: Theory of the Condensed State* Vol. 9 (Elsevier, 2013).